Optimization of a residential district with special consideration on energy and water reliability[1]

Pietro Elia Campana[a*] , Steven Jige Quan[b,c], Federico Ignacio Robbio[d], Anders Lundblad[a,e], Yang Zhang[e], Tao Ma[f], Björn Karlsson[a], Jinyue Yan[a,e]

[a]School of Business, Society & Engineering, Mälardalen University, Box 883, Västerås SE-72123, Sweden

[b]Sino-U.S. Eco Urban Lab, College of Architecture, Georgia Institute of Technology, North Avenue, Atlanta GA 30332, USA

[c]Sino-U.S. Eco Urban Lab, College of Architecture and Urban Planning, Tongji University, Shanghai 200092, China

[d]ABB AB, Tvärleden 2, Västerås SE-72159, Sweden

[e]School of Chemical Science & Engineering, KTH Royal Institute of Technology, Teknikringen 42, Stockholm SE-10044, Sweden

[f]Institute of Refrigeration and Cryogenics, Shanghai Jiao Tong University, Shanghai 200240, China

Abstract

Many cities around the world have reached a critical situation when it comes to energy and water supply, threatening the urban sustainable development. From an engineering and architecture perspective it is mandatory to design cities taking into account energy and water

[1]The short version of the paper was presented at CUE2015 on Nov. 15-17, Fuzhou, China. This paper is a substantial extension of the short version with original paper title, "Spatial optimization of residential urban district - Energy and water perspectives" and Paper No. 167.

*Corresponding author: pietro.campana@mdh.se

issues to achieve high living and sustainability standards. The aim of this paper is to develop an optimization model for the planning of residential urban districts with special consideration of renewables and water harvesting integration. The optimization model is multi-objective which uses a genetic algorithm to minimize the system life cycle costs, and maximize renewables and water harvesting reliability through dynamic simulations. The developed model can be used for spatial optimization design of new urban districts. It can also be employed for analyzing the performances of existing urban districts under an energy-water-economic viewpoint.

The optimization results show that the reliability of the hybrid renewables based power system can vary between 40 and 95% depending on the scenarios considered regarding the built environment area and on the cases concerning the overall electric load. The levelized cost of electricity vary between 0.096 and 0.212 \$/kWh. The maximum water harvesting system reliability vary between 30% and 100% depending on the built environment area distribution. For reliabilities below 20% the levelized cost of water is kept below 1\$/m^3 making competitive with the network water tariff.

Keywords: Optimization, genetic algorithm, renewable energy, hybrid power systems, water harvesting, residential urban districts.

1 Introduction

According to the World Health Organization, more than half of the current world's population (53%) lives in urban areas [1], whereas the United Nations forecasts project that 6.3 billion people are going to live in cities by 2050 [2]. Thus, the sustainability of cities around the world is threatened by the growing demand for energy, water and food supplies. The urban water-energy-food nexus development requires an integrated design process that comprises not only policies but also technical solutions [3]. From an engineers and architects point of view, the above mentioned statistics put a lot of pressure on how to design our modern and future cities. The aim of this paper is to analyse the integration of renewable hybrid power systems and water harvesting technology into the urban environment as sustainable solutions for high urban water and energy self-sufficiency. In particular, this study aim at analyse the reliability of renewables and water harvester compared to electricity and water loads in a residential district.

Hybrid power systems have been studied thoroughly especially for off-grid applications. Ma et al. studied the optimal integration of solar, wind and hydro pumped storage systems for a few hundred kW microgrid in a remote island in Hong Kong [4]. The authors concluded that for an optimal design of a standalone hybrid power supply system, the combination of wind and solar energy is essential [5]. Using a particle swarm optimization algorithm, Shang et al. studied the optimal size of the battery capacity in solar/wind/diesel standalone hybrid power system for a tropical island near Singapore [6]. The authors focused in particular on optimal dispatch of the stand-alone system to minimize the operation costs and at the same time increase the penetration level of renewables. Gan et al. developed a software tool for sizing off-grid hybrid renewable energy systems using a location in Scotland as a case study [7]. The developed tool was intended to support project management in evaluating the batteries and diesel generator capacities based on the renewable available resources both for short and long term operation using a life cycle cost approach. Maleki and Pourfayaz studied the optimization of hybrid renewables based power system for a specific site in the South of Iran [8]. In particular the authors focused on the evaluation of different evolutionary algorithms for optimum sizing of a solar/wind/battery hybrid system to meet the load demand while minimizing the total annual cost and loss of power supply probability.

The integration of hybrid power systems into on-grid areas as distributed generation system has become a recent research topic for high energy performances buildings. González et al. studied the optimization of a grid-connected hybrid renewables based power system compared to a given electricity demand for case study in Catalonia [9]. Using particle swarm optimization, García-Triviño et al. studied the optimal power control of a grid-connected inverter supplied from a solar/wind hybrid power system equipped with battery and hydrogen storage systems [10].

Lu et al. presented a comprehensive review on the design and control approaches of the nearly/net zero energy building highlighting the lack of optimal design and control strategies [11]. Carlucci et al. presented a multi objective optimization model for the design of a detached net zero-energy house located in the South of Italy to minimize thermal and visual discomfort using uses the non-dominated sorting genetic algorithm [12]. The authors highlighted the importance of using complex optimization problems with many objective functions to assess the effects of a large number of available building variants. Lu et al. compared the optimal design of buildings using single objective and multi objective optimization using genetic algorithm for two case studies [13]. The authors concluded that optimization of buildings with renewable energy systems can lead to better performances than the benchmark building considered in their study. Moreover, the authors verified that single objective optimization can provide the best solution while multi objectives optimization can guide designers for better trade-off solutions. Using distributed energy system for meeting the energy demand, Lu et al. proposed a multi-objective optimization approach based on genetic algorithm for a net-zero exergy district in Hangzhou, China [14]. The optimization model was to minimize the e life cycle cost of the system and at the same time maximize the exergy efficiency including twelve energy supply systems to provide power and heat. The optimization model was based on the operation time of each energy supply technology.

Similarly, rainwater harvesting systems assessment and optimization have been conducted as technical solution to face the exacerbation of water issue in urban areas. Mehrabadia et al.

assessed the residential rainwater harvesting efficiency to meet non-drinkable water demands in three different Iranain cities marked out by different climate conditions (Mediterranean, humid and arid climate) [15]. The study concluded that the tank capacity is a key factor to consider for maximizing rainwater storage, the optimal water tank is striclty dependent on precipitation amount and roof area, and rainwater harvesting efficiency is dependent on climate. Hashim et al. focused on simulations and optimization of large scale rainwater harvesting [16] describing a new designing technique. The optimization model was based on the minimization of the total system costs including supplemental cost for the utility water to meet the water demand. The conducted simulations showed that roof area and water demand are the main key factors affecting the storage tank size. Chiu et al. proposed an optimization approach for rainwater harvesting systems with special consideration of energy-saving approach for hilly communities [17]. Using a water-energy nexus approach, the authors conluded that rainwater harvesting systems are both a water-saving method and also an energy-saving technique for hilly location.

Compared to previous studies, as far as the authors are aware, the novelty of the present work is to develop a general optimization tool to study the optimal integration of hybrid power systems and water harvesting techniques in the urban environment in order to achieve high sustainability standards. This tool allows to study the reliability of renewables equipped with energy storage and water harvesting system in residential districts compared to electricity and water loads, respectively. A novel aspects of the paper is to analyse the interrelation between water and power mainly assuming ground mounted photovoltaic systems as water harvesting area. A further novel aspect of the optimization tool is using a spatial perspective rather than a power and water harvester systems perspective used in previous research works to optimize the match between energy and water demand, and supply. The optimization model finds the optimal area distribution within 1 km^2 between the built environment area, and area for the installation of renewables, taking into account that part of the residential district area is used as urban leisure area and for the road network. The model considers the following renewables and energy storage system: building integrated photovoltaic systems (function of the built environment area), ground mounted photovoltaic systems, wind turbines and battery storage system. The water harvesting system comprises the harvesting area, assumed equal to the roof area (function of the built environment area), the effective ground mounted photovoltaic area, and the water tank. The optimization model is based on annual hourly dynamic simulations of the renewables, energy and water storage systems. A typical residential district of Gothenburg, Sweden, is taken as case study to identify the main built environment area parameters.

The developed model can be used for the design of new urban districts or to evaluate the performances and provide suggestions for existing urban districts under an energy, water and economic viewpoints to promote renewables and water harvesting integration. It has to be pointed out that the developed tool represents a general integrated model that can be applied for energy and water harvesting performances everywhere and for different types of district, and it can thus represents a handy instrument for engineers, architects and urban planners.

This paper is organized as follows: section 2 deals with the methodology applied in this study and in particular with the developed optimization model based on the simulation of several sub-models, such as building, photovoltaic power, wind power, battery state of charge, and water harvester state of fill; in section 3, the results of the optimization are presented and discussed; in section 4 the outcomes of this study are summarized and the directions for future studies are discussed.

2 Methodology

In a typical residential km^2 there can be a combination of different areas with different intended uses, proportions and layouts as shown in Figure 1 as a conceptual framework. The built environment area determines the electric and water consumption profiles depending on the number of dwelling units in a given area. At the same time, the built environment area put constraint on the building integrated PV area. In this study we have considered half of the roof is used to install building integrated PV system. Similarly, the building integrated water harvesting area is function of the built environment area since it has been assumed that the entire roof is used to collect rainwater. The water harvesting area is also function of the area for the installation of ground based PV systems. In this study we have assumed that the effective ground based PV systems area is used as a further water harvesting area. The green-leisure area and area occupied by the road network have been set equal to 10% of the entire km^2 and 10% of the built environment area, respectively. These assumptions have been made based on the photointerpretation of a typical residential district in Gothenburg, as shown in Figure 2. The same approach has been used to evaluate the building and garden areas for a typical residential house. The area for the installation of ground based PV takes into consideration a land use factor (defined as the ratio between solar panels area and total area) of 33% due to the high latitude of Gothenburg. The wind turbine area refers to the acoustic influence areas of each installed wind turbine. The acoustic influence area has been calculated from the sound pressure level of the generator assuming to keep the noise emissions below 40 dB according to the Swedish regulations [18]. The battery balances the mismatch between energy production and consumption. The electric grid is considered as back-up for the PV-wind-battery system while the dumped power production is assumed to be injected into the grid. Similarly, the water harvester balances the mismatch between water harvested and consumed. A schematic diagram of the hybrid power/water harvesting system investigated is given in Figure 3.

The optimization process finds the optimal area distribution that minimize the life cycle costs (LCC) of hybrid and water harvesting systems and at the same time maximizes their reliability. The decisional variables of the optimization problem are the following: built environment area (used as sensitive parameters), ground based PV system area, wind turbine area, battery and water harvester capacities. The current version of the model allows to optimize the areas distribution but it does not provide any information regarding the spatial location of the decisional variables. The weather data in for the selected location, including the global horizontal radiation (W/m^2), the diffuse horizontal radiation (W/m^2), wind speed (m/s), ambient temperature (°C), precipitation (mm) and snow depth (mm), is taken from a global climatic database, Meteonorm [19].

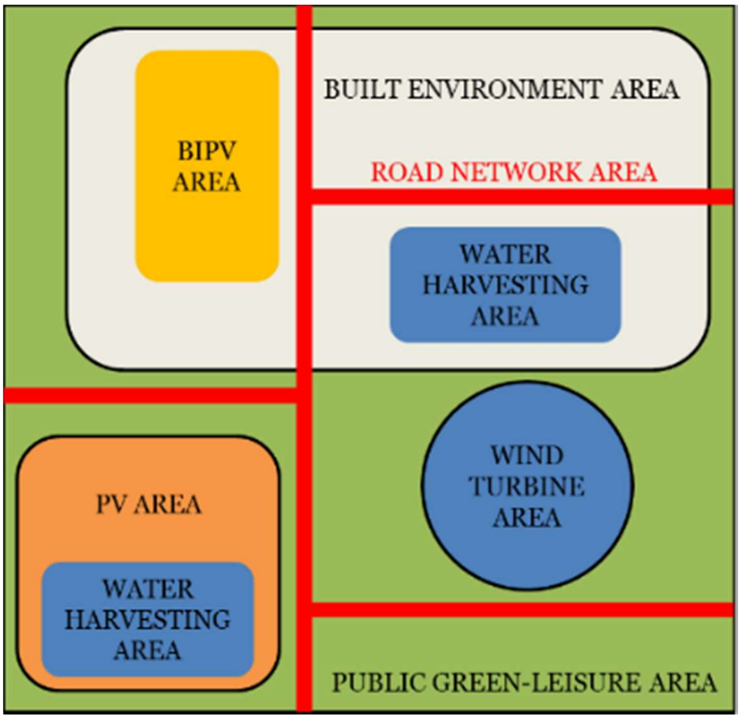

Figure 1: Conceptual framework of 1km^2 residential district.

Figure 2: Photointerpretation of a residential area.

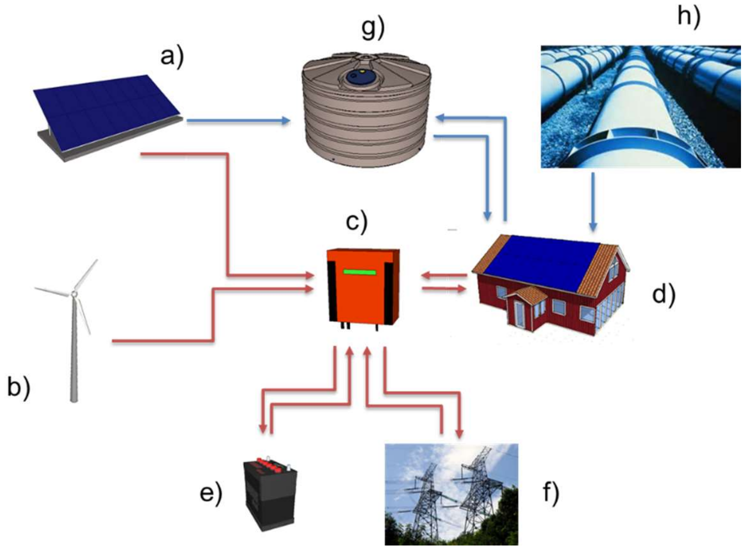

Figure 3: Hybrid power/water harvesting system schematic layout (a) ground mounted PV system; b) wind power system; c) power conditioning system; d) household; e) battery storage system; f) electric grid; g) water harvester; h) water network).

2.1 Optimization model

The optimization problem finds the optimal area distribution (among built environment area, ground based PV system area, wind turbine area) that minimize the *LCC* of the renewable based hybrid power system LCC_{ren} and the *LCC* of the water harvesting systems LCC_{whs} and at the same time maximizes their reliability, R_{ren} and R_{whs} respectively, and minimize the surplus of power injected into the grid *S*, that means maximizing the renewable power self-consumption. R_{ren} represents the hours during which the power consumption is met by the renewables power production (equipped with the battery storage system). Similarly, R_{whs} refers to the number of hours the water consumption is covered by the water harvesting system. The mathematical formulation of the proposed optimization approach is given by the following set of equations:

$$min(LCC_{ren}) \tag{1}$$

$$min(LCC_{whs}) \tag{2}$$

$$max(R_{ren}) \tag{3}$$

$$max(R_{whs}) \tag{4}$$

$$min(S) \tag{5}$$

$$constraints \begin{cases} BEA = 25, 50, 75\%\ of\ 1km^2 \\ 0 \leq PVA \leq 0.75\ km^2 \\ 0 \leq WTA \leq 0.75\ km^2 \\ BEA + PVA + WTA + RNA + GLA = 1km^2 \\ RNA = 12\%\ BEA \\ 0 \leq BC \leq 10\ MWh \\ 0 \leq WHC \leq 4000\ m^3 \end{cases} \tag{6}$$

Where, *BEA* stands for built environment area, *PVA* for ground mounted PV systems area, *WTA* for wind turbine area, *RNA* for road network area, *GLA* for green-leisure area, *BC* for battery capacity, and *WHC* for water harvester capacity. The LCC_{ren} comprises the life cycle cost of the ground based PV systems LCC_{pv}, building integrated PV systems LCC_{bipv}, wind turbine LCC_{wt}, battery LCC_{batt}, and electricity taken from the electric network to meet the load LCC_{en} At the same time the LCC_{ren} takes into account the life cycle revenues *LCC* due to carbon tax

LCC_{ct} that penalizes the electricity taken from the grid, and electricity surplus generated by the hybrid power system and fed into the grid LCR_{es}. The LCC_{whs} comprises the life cycle cost of the water harvester and related installations LCC_{wh}, and the water taken from the water network LCC_{wn}. The LCC_{ren} and LCC_{whs} are calculated by the following equations [20, 21]:

$$LCC_{ren} = ICC_{ren} - \sum_{n=1}^{N} \frac{d_t}{(1+i)^n} tr + \sum_{t=1}^{N} \frac{a_t}{(1+i)^n}(1-tr) - \frac{s}{(1+i)^n} \quad (7)$$

$$LCC_{whs} = ICC_{whs} - \sum_{n=1}^{N} \frac{d_t}{(1+i)^n} TR + \sum_{t=1}^{N} \frac{a_t}{(1+i)^n}(1-TR) - \frac{s}{(1+i)^n} \quad (8)$$

Where, ICC_{ren} is the initial capital cost of the renewables based system (US$), ICC_{whs} is the initial capital cost of the water harvesting system (US$), N is the lifetime of the project (years), d_t is the annual depreciation (US$), i is the interest rate (%), tr is the tax rate (%), a_t is the annual costs (US$), and s is the salvage value (US$). N, i, and tr have been set equal to 30 years, 1%, and 22% [22]. The depreciation has been assumed straight-line and salvage value equal to 10% of the ICC [18]. LCC_{ren} and LCC_{whs} are given by the following equations:

$$LCC_{ren} = LCC_{pv} + LCC_{bipv} + LCC_{wt} + LCC_{batt} + LCC_{en} + LCC_{ct} - LCR_{es} \quad (9)$$

$$LCC_{whs} = LCC_{wh} + LCC_{wn} \quad (10)$$

The optimization model is based on hourly dynamic models of the building energy demand, PV system, wind turbine, battery and water harvesting system charge and discharge. The decision variables of the optimization model include: (I) the ground mounted PV area; (II) the wind turbines area; (III) the battery capacity (MWh); and the water harvester capacity (m^3). The built environment area has been considered as a sensitive parameters and varied in the range 25% to 75% of the entire 1 km^2. The economic parameters used in the optimization model are listed in Table 1.

Table 1: Economic parameters affecting the LCC function.

LCC_{pv} (US$/$W_p$)	2.7
LCC_{bipv} (US$/$W_p$)	3.6
LCC_{wt} (US$/$W_r$)	2.4
LCC_{batt} (US$/Wh)	3.1
LCC_{wts} (US$/$m^3$)	1500
LCC_{en} (US$/kWh)	4.4
LCR_{es} (US$/kWh)	1.1
LCC_{wn} (US$/$m^3$)	3.6

The LCC have been calculated from the ICC considering fixed annual maintenance costs and replacement costs of the main components. The renewables ICC have been taken from the 2015 IRENA (International Renewable Energy Agency) report on renewable power generation costs in 2014 and refer to the average installation costs for residential and utility scale projects [23]. The ICC of residential PV systems, ground mounted PV systems and wind turbine have been set equal to 2500 US$/$kW_p$, 2000 US$/kW_p, and 1700 US$/kW. As regards PV systems, the Swedish government has promoted the installation of grid connected PV systems with supporting policies since 2005 [24]. In 2016, the overall government investment will account for 225 million SEK (approximately 27 million US$). Since the 1st January 2015, the supporting scheme compensates 30% of the grid connected PV system investment costs for commercial companies, and 20% for individual homeowners. The highest subsidy is 1.2 million SEK (approximately 150,000 US$) and the eligible costs may not exceed 37 000 SEK (approximately 4,500 US$) plus VAT per installed kW_p [25]. In calculating the LCC of residential and ground mounted PV systems, we have not considered any subsidy, whereas in calculating the levelized cost of electricity (LCOE) we have analysed the effects of considering or not the subsidy. The annual operation and maintenance cost have been conservatively set equal to 2% of the ICC.

The replacement costs are mainly for the inverter, assumed to be replaced every 10 years, and are equal to 450 US$/kW for residential systems and 250 US$/kW for larger scale systems [26]. The LCC of the battery have been calculated assuming a specific ICC of 700 US$/kWh (Li-on battery pack) [27], an annual maintenance costs equal to 5% of the ICC, and replacements every 7 years. The LCC of the water harvesting system have been calculated from the ICC and operating costs given in Gurung et Sharma [28]. The electricity price for domestic consumers including all taxes and levies for Sweden is 0.185 €/kWh (0.21 US$/kWh) [29]. In this study, it has been assumed that the surplus of electricity generated by the renewables can sold to the electric grid at a price of 0.05 US$/kWh considering both spot price and green certificates [30]. Green certificates are also the only incentives to support wind power projects [31].

The water tariff for Gothenburg has been taken equal to 14.1 SEK/m^3 (1.7 US$/m^3) [32].

The levelized cost of electricity and water, LCOE and LCOW, have been calculated according to the following equations [20, 21]:

$$LCOE = \frac{LCC_{pv} + LCC_{bipv} + LCC_{wt} + LCC_{batt}}{EP \sum_{n=1}^{N} \frac{r_t}{(1+i)^n}} \tag{11}$$

$$LCOW = \frac{LCC_{wh}}{WH \sum_{n=1}^{N} \frac{r_t}{(1+i)^n}} \tag{12}$$

Where, *EP* is the annual energy production (kWh), *WH* is the annual water harvested (m^3), and r_t is the degradation rate (%). r_t for the renewables based system has been assumed equal to 1% considering mainly the photovoltaic system degradation, while it has been assumed 0% for the water harvesting system.

The optimization process is based on hourly dynamic models of the building energy requirements, PV system and wind turbine power production, and battery and water harvesting system charge and discharge. The optimization model is implemented in Matlab R2015b using GA in the Global Optimization Toolbox. As a well-recognized optimization technique, genetic algorithm GA has been used to solve the complex engineering optimization problem [33-37]. *GA* is an advanced search and optimization technique, developed by Holland [38] to imitate the process of natural selection. The main advantage of GA compared to traditional optimization methods is the reliability, accuracy and convergence speed in finding global optimal solutions in multi-objectives non-linear optimization problems [39, 40]. The settings of the GA optimization parameters are listed in Table 2. A schematic flowchart of the optimization process is given in Figure 4. The optimization model is based on an open-source code, OptiCE [41].

Table 2: Genetic algorithm set parameters [42].

.Generations	800
Population size	50
Algorithm	Variant of NSGA II
Crossover function	Heuristic
Crossover rate (%)	50
Mutation function	Uniform
Mutation rate (%)	5

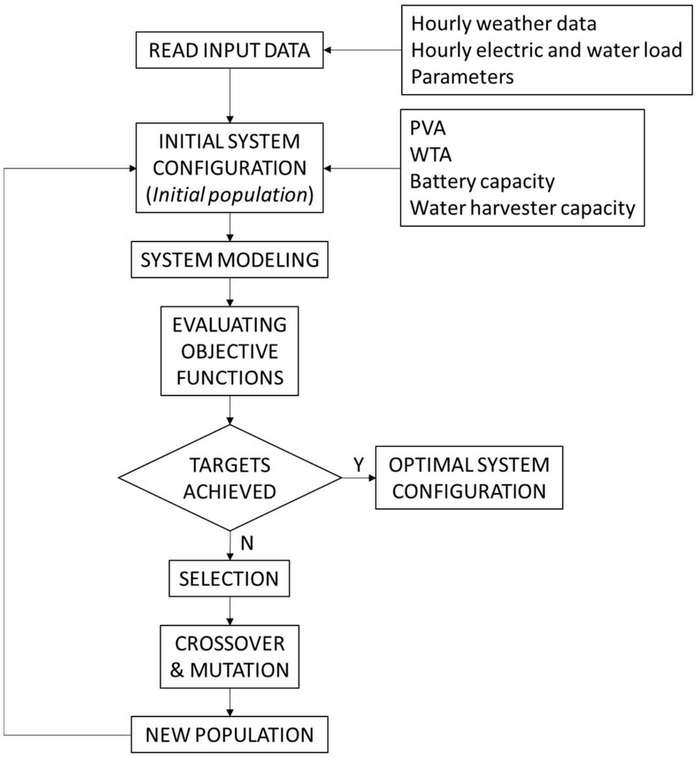

Figure 4: Optimization process flowchart.

2.1.1 Building model

In this study we assumed that the built environment area of the residential district is structured into typical Swedish single family houses with five occupants, a model of which is shown in Figure 5. The simulated building has a living space of 200 m^2 distributed in two floors of 3 meters height each. The temperature is kept constant at 20 ºC. The electric load of the building refers mainly to two different contributions: the first due to the electric consumption for appliances, lighting and water pumping; and, the second concerning the heat pump requirements for space heating and cooling, and domestic hot water. The electric consumption for appliances, and lighting, refers to measured data of a single family house with five occupants retrieved from Polysun database [43]. The electric consumption for pumping the harvested water volume has been calculated assuming an electric pump with an overall efficiency of 60%. The electric demand of the heat pump has been calculated from the thermal energy demand using an empirical relationship between ambient temperature and heat pump coefficient of performance *COP* [44].

Figure 5: Swedish typical residential single family house.

The thermal energy demand for space heating and cooling purposes $Q_{h\&c}$ (W) has been calculated through the heating/cooling energy balance equation given by [45]:

$$Q_{h\&c} = HL - HG + Mc_{p,b}\frac{dT}{dt} \tag{13}$$

where, *HL* is the heat losses (W), *HG* is the heat gain (W), *M* is the mass of the building (kg), $c_{p,b}$ is the building specific heat capacity (Wh/(kg·ºC)), d*T* is the building hourly temperature variation (ºC), and *dt* is the time step (hour). The heat losses parameter takes into account the losses due to transmission HL_t (W), ventilation HL_v (W), and infiltration HL_i (W). *HG* takes into account the heat gains (W). The heat gains caused by people, lighting system, and appliances have not been considered in this study due to their unpredictability in modelling. Similarly, the heat gains due to solar radiation have been omitted since depend on the specific orientation of the building and on the arrangement of the windows area. Moreover, we have assumed to keep constant the internal building temperature setting dT/dt equal to zero. It has to be pointed out that the building model used in this study is for providing an accurate overview of the residential district energy consumption for space heating and cooling rather than a detailed analysis of the energy consumption of the single buildings. Due to the assumptions made, the results provide the worst case scenario in terms of building energy demand. HL_t, HL_v, and HL_i, are given by the following set of equations:

$$HL_t = U \cdot A \cdot (T_{in} - T_{out}) \tag{14}$$

$$HL_v = (1-\alpha) \cdot n_v \cdot V_v \cdot \rho_a \cdot c_{p,a} \cdot (T_{in} - T_{out}) \tag{15}$$

$$HL_i = n_i \cdot V_i \cdot \rho_a \cdot c_{p,a} \cdot (T_{in} - T_{out}) \tag{16}$$

Where, U is the overall heat transfer coefficient of the building (W/(m^2·ºC)), A is the total surface area of the building (m^2), T_{in} is the set indoor temperature (ºC), T_{out} is the outdoor temperature (ºC), α is the heat recovery efficiency (%), n_v is the ventilation air changes per hour (1/h), n_i is the infiltration air changes per hour (1/h), V_v is the building ventilated volume (m^3), V_i is the building infiltrated volume (m^3), ρ_a is the air density (kg/m^3), $c_{p,a}$ is the air specific heat (Wh/(kg·ºC). The daily average thermal energy demand for domestic hot water Q_{dhw} (W) has been calculated with the following equation:

$$Q_{dhw} = \rho_w \cdot c_{p,w} \cdot V_{d,p} \cdot (T_h - T_c) \tag{17}$$

where, ρ_w is the water density (kg/m^3), $c_{p,w}$ is the water specific heat (Wh/(kg·ºC), $V_{d,p}$ is the daily volume of hot water per person (m^3), T_h and T_c are the hot and cold water temperatures (ºC). In this study, we assumed that the daily volume of hot water per person is equal to 70 l, and the hot and cold water temperatures are 55 and 10 ºC, respectively. The empirical relationship between ambient temperature and heat pump COP used to calculate the heat pump electricity consumption is the following [44]:

$$COP = 2.79 + 0.036 \cdot T_{out} + 0.0006036 \cdot {T_{out}}^2 \tag{18}$$

The main building simulation parameters are summarized in Table 3.

Table 3: Building simulation parameters.

Parameter	Normal building	Passive house
U (W/(m^2·°C))	0.5	0.13
T_{in} (C)	20	20
α (%)	0	50
n_v (1/h)	0.4	0.4
n_i (1/h)	0.6	0.3
SHGC (%)	50	50
WWR (%)	50	50

To analyse the effects of building insulation on the electricity requirements of the heat pump for space heating, two different U-values have been chosen: 0.13 and 0.5, respectively. The former refers to the typical U-value of a passive building for a single family house, while the latter refers to the typical U-value of a normal building single family house [43].

2.1.2 Photovoltaic model

The area for the installation of PV system comprises both the area for BIPV, assumed equal to half of the reference building roof, and the area for the installation of ground based PV systems. As regards the second typology, a ground area occupation ratio (defined as the ratio between solar panels area and total area) of 33%, corresponding to a pitch distance between photovoltaic rows of 9 m, has been assumed as guideline value to minimize the mutual shading between each row in Sweden. The assumption that all the building have a roof pitch south facing. The hourly power output from the PV system P_{PV} (W) is given by [46]:

$$P_{PV} = \eta_{PV} A_{PV} G_{g,t} \tag{12}$$

Where, η_{PV} is the efficiency of the PV module (%), A_{PV} is the PV array area (m2), and $G_{g,t}$ is the global solar radiation on the tilted surface. In this study we have assumed an optimal tilt angle of 60° to maximize the solar energy harvested during the winter period, typically, the period when most of the energy consumption is concentrated. η_{PV} is given by the following equation [46]:

$$\eta_{PV} = \eta_{PV,STC}\left[1 + \frac{\mu}{\eta_{PV,STC}}(T_a - T_{STC}) + \frac{\mu}{\eta_{PV,STC}}\frac{(NOCT - 20)}{800}(1 - \eta_{PV,STC})G_{g,t}\right] \quad (13)$$

Where, $\eta_{PV,STC}$ is the efficiency of the PV module at standard test conditions (STC), μ is the temperature coefficient of the output power (%/°C), T_a is the ambient temperature (°C), T_{STC} is the standard test conditions temperature (25°C) and *NOCT* is the nominal operating cell temperature (°C). A summary of the simulated PV modules characteristics is given in Table 4.

Table 4: Characterizing parameters of the PV module (Yingli 260 W_p polychristalline) [47].

I_{mp} (A)	8.4
V_{mp} (V)	30.8
I_{sc} (A)	9.0
V_{oc} (V)	38.2
Area (m²)	1.62
$\eta_{PV,STC}$ (%)	16.02
μ_{Voc} (V/°C)	-0.129
NOCT (°C)	42

2.1.3 Wind power model

In the optimization model, the wind turbine area refers to the sum of the acoustic influence areas of each installed wind turbine. A 30 kW_r wind turbine model Jimp30 mounted on a 30 meters tower has been chosen as reference generator to be easily integrated in residential areas [48]. The acoustic influence area has been calculated from the sound pressure level of the generator assuming to keep the noise emissions below 40 dB according to the Swedish regulations [49]. Assuming a hemispherical noise propagation, the sound pressure level L_p (dB) at a distance r (m) from the wind turbine is given by [18]:

$$L_p = L_{wt} - 10\log_{10}(2\pi r^2) - \alpha r \tag{14}$$

Where, L_{wt} is the sound pressure level of the wind turbine, and α is the sound absorption coefficient assumed equal to 0.005 dB/m [18]. L_{wt} as been set equal to 88 dB, as derived from the wind turbine manufacturere company. The corresponding influence area to meet the noise pollution requirements is 25000 m^2. The model of the hourly power output from the wind turbine power system P_{WT} (W) is given by the following relationship [50]:

$$P_{WT} = \begin{cases} P_r \frac{v^k - v_i^k}{v_r^k - v_i^k} & (v_i \le v \le v_r) \\ P_r & (v_r \le v \le v_o) \\ 0 & (v < v_i \text{ and } v > v_o) \end{cases} \tag{15}$$

where, P_r is the rated power (W), k is the velocity-power proportionality assumed equal to 3 [51], v_i, v_r and v_o are the cut-in, rated and cut-out characteristic speeds of the wind power curve (m/s), respectively. The wind speed v (m/s) at the hub height has been calculated using the wind profile power law relationship assuming a roughness coefficient of 0.14 [18]. v_i, v_r and v_o have been set equal to 3.5, 11 and 20 m/s, respectively [48].

2.1.4 Battery model

The battery is used in the optimization model to manage the mismatching between power production and load. The model calculates the hourly state of charge of the battery SOC_{bat} (Wh) according to the following two equations, for charging and discharging processes, respectively [52]:

$$SOC_{bat}(t) = SOC_{bat}(t-1)(1-\sigma_{sd}(t)) + \left[E_{pro}(t) - \frac{E_{load}(t)}{\eta_{inv}}\right]\eta_b(charging) \quad (16)$$

$$SOC_{bat}(t) = SOC_{bat}(t-1)(1-\sigma_{sd}(t)) + \left[\frac{E_{load}(t)}{\eta_{inv}} - E_{pro}(t)\right](discharging) \quad (17)$$

where, σ_{sd} is the hourly self-discharge rate, E_{pro} is the hourly energy produced from PV and wind turbine systems (Wh), E_{load} is the hourly load energy requirement (Wh), η_{inv} is the inverter efficiency (%), and η_b is the battery bank efficiency (%). The SOC is constrained to vary between SOC_{min} and SOC_{max}. The efficiency of the discharging process has been assumed equal to 100% [53]. The characteristic parameters of the battery model have been summarized in Table 5.

Table 5: Characteristic parameters of the battery model [53].

σ_{sd} (%)	0.02
η_c (%)	80
η_{inv} (%)	90
SOC_{min} (%)	20
SOC_{max} (%)	100

The procedure adopted by the optimization model to design the optimal battery capacity is to vary the battery capacity (a decisional variable of the optimization model) every optimization step to match energy consumption and production and to pursue two objective functions: maximize the reliability of the renewables R_{ren} and at the same time minimize the life cycle cost LCC_{ren}. Every optimization step the entire energy system is simulated hour by hour and the objective functions are calculated.

2.1.5 Water harvesting model

Similarly to the battery model, the water harvesting model computes the state of fill of the water harvester SOF_{wh} depending on the water harvested and water demand according to the following equations:

$$SOF_{wh}(t) = SOF_{wh}(t-1)(1-\sigma_{eva}) + [W_{harveste}\ (t) - W_{load}(t)](charging) \quad (18)$$

$$SOF_{wh}(t) = SOF_{wh}(t-1)(1-\sigma_{eva}) + [W_{load}(t) - W_{harvested}(t)](discharging) \quad (19)$$

Where, σ_{eva} represent the water losses due to evaporation assumed equal to 0% due to the latitude of the site chosen, $W_{harvsted}$ is the water volume harvested (m^3), and W_{load} is the water volume demand (m^3). The water harvested comprises both the water from precipitation both the water from snow melting assuming an average conversion ratio between snow and precipitation equal to 10%. The water load has been assumed equal to 1000 litres per day assuming five occupants and a specific water consumption of 200 litres per person and day [32]. Typically, the water household consumption can be apportioned in the following manner: 10 litres for drinking and food, 40 for flushing the WC, 40 for dish-washing, 30 for laundry, 70 for personal hygiene, and 10 litres per person and day for other uses. Since the LCC_{whs} refers to a water harvesting system equipped with sanitation device, in this study we assumed to use the all harvested water with a comparable quality of the municipal water network. The municipal water network is assumed as a back-up system. The load profile has been assumed constant. Similarly to the battery system, the design of the optimal water harvesting capacity is carried out during the optimization process by varying the water harvesting capacity (a decisional variable of the optimization model) every optimization step to match water supply and demand. Every optimization step the water harvesting system is simulated hour by hour to maximize its reliability REL_{whs} and at the same time minimize the LCC_{whs}.

2.2 Evaluated scenarios and cases

In this study, we have evaluated three different scenarios based on the density of the residential district. In particular, we have considered the built environment area to change between 25%, 50%, and 75% of the entire km^2, namely S1, S2, and S3 respectively. Moreover, we have considered three different cases based on the load covered by the hybrid power system: a) the electric load refers only to the electric load of the household electric appliances and water pumping, namely C1; b) the electric load refer to the electric load of the appliances plus the electric load for domestic hot water and space heating and cooling assuming a building U-value of 0.13 ($W/(m^2 \cdot {}^{o}C)$), namely C2; and c) the electric load refer to the electric load of the appliances and water pumping plus the electric load for domestic hot water and space heating and cooling assuming a building U-value of 0.5 ($W/(m^2 \cdot {}^{o}C)$), namely C3.

3 Results and discussions

3.1 Climatic data

The main climatic parameters affecting the hybrid power system and water harvesting system operation are shown in Figure 6. Gothenburg is marked out by an annual global solar irradiation of 957 kWh/m^2, mostly concentrated between March and October. The annual average wind speed and precipitation is 2.6 m/s at 10 m height and 704 mm, respectively. The average annual snow depth is 32 mm and mainly distributed between December and March.

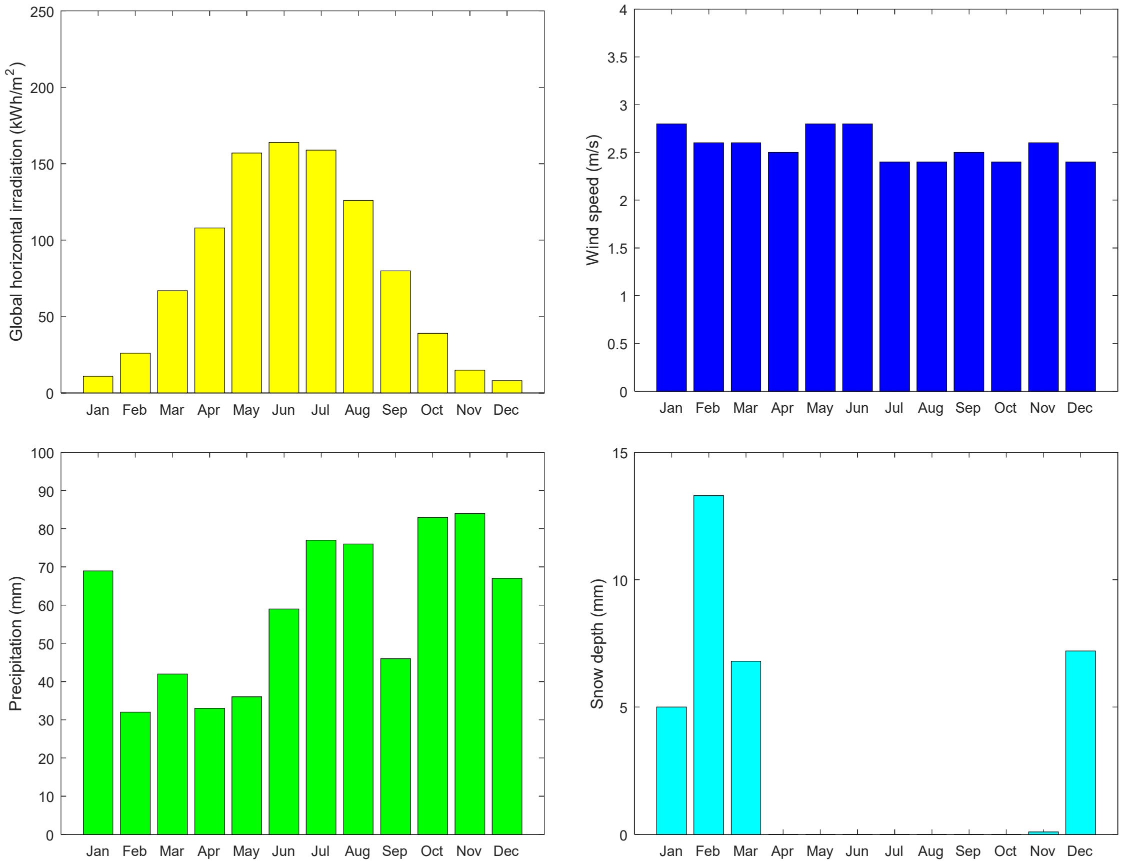

Figure 6: Climatic data affecting the operation of hybrid power system and water harvesting system for Gothenburg.

3.2 Electric and thermal demand and supply

The profiles of the electric loads for appliances, and heat pump to cover the thermal demand of domestic hot water and space heating and cooling is depicted in Figure 7. The space heating and cooling load refers to the studied reference building marked out by a U-value equal to 0.5 W/(m^2·ºC). The difference in the electric load of the heat pump for space heating and cooling for different U-values, 0.13 and 0.5 W/(m^2·ºC), is depicted in Figure 8. The annual energy consumption for space heating and cooling is 11.1 down and 4.48 MWh/year for the high and low U-value building, respectively. The space heating and cooling loads refer to the electricity consumption of the heat pump. The heat pump space heating and cooling consumption has been calculated from the thermal energy demand of the household using Equation 18 (heat pump

COP). A summary of the heating and cooling demand of the heat pump for the entire district as a function of scenarios and building type is provided in Table 6.

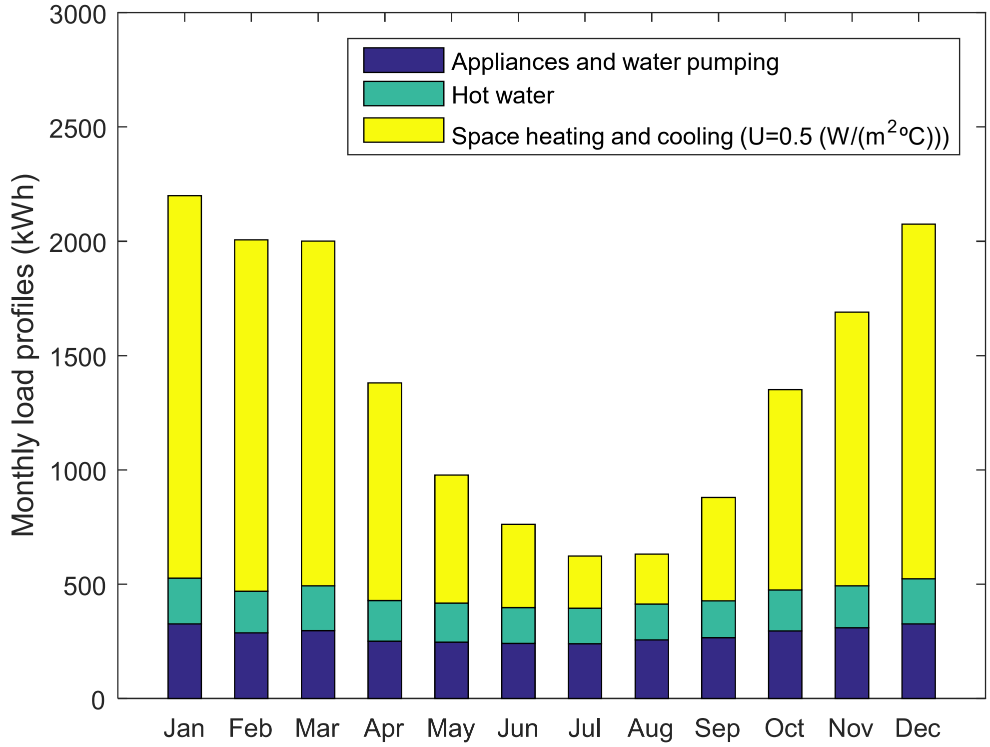

Figure 7: Electricity monthly load profile.

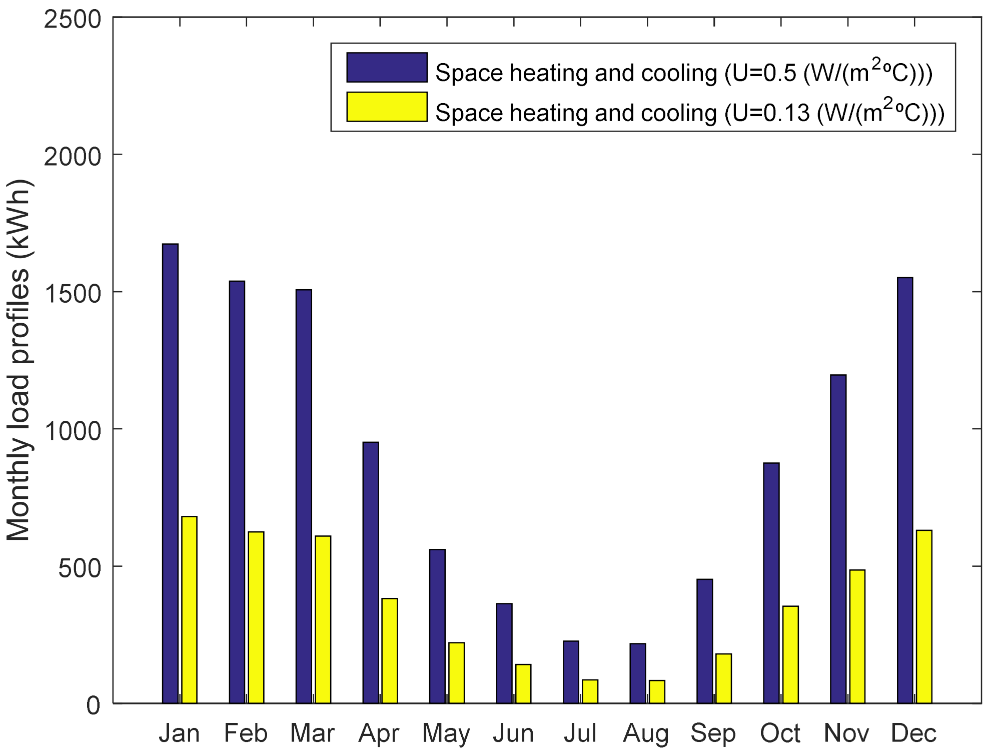

Figure 8: Electricity monthly load profile for space heating as a function of the overall building U-value.

Table 6: Heat pump electricity consumption as a function of scenarios and building type (GWh).

Scenario	Normal building (U-value=0.5 W/(m^2·°C))	Passive building (U-value=0.13 W/(m^2·°C))
S1	4.62	1.86
S2	9.25	3.73
S3	13.88	5.60

A summary of the hourly specific electricity production (kWh/kW) for an entire year from the chosen small wind turbine model and PV system is depicted in Figure 9.

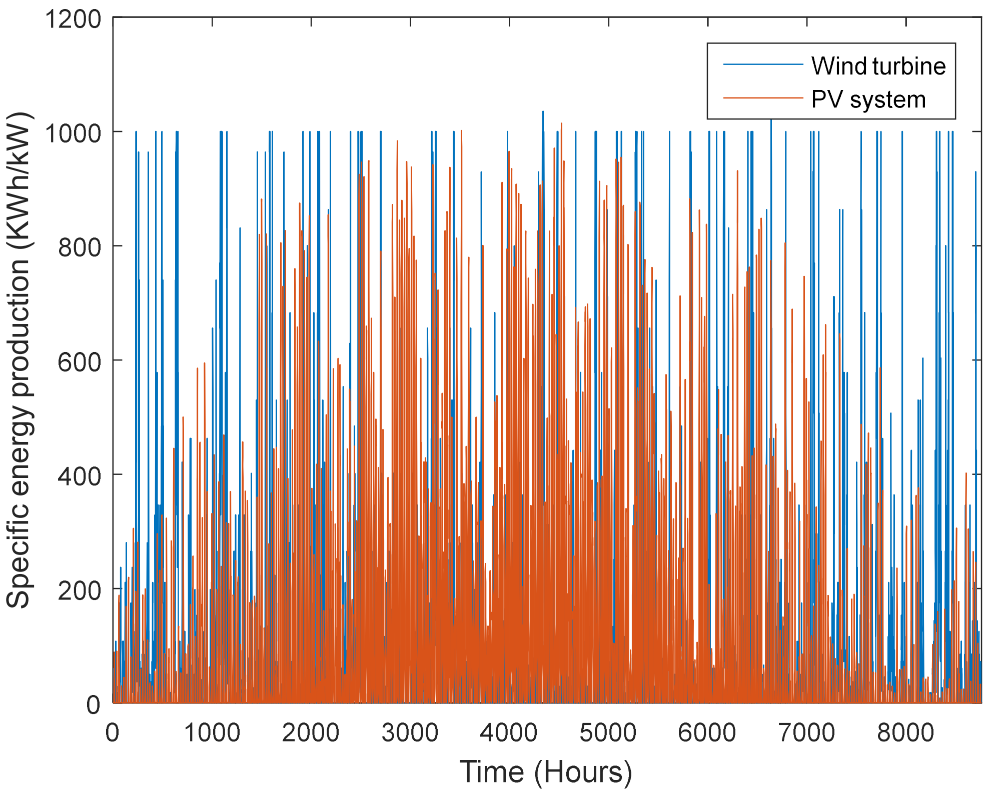

Figure 9: Specific energy production per installed kW of wind turbine and PV system in Gothenburg.

As it can be seen from Figure 9, the pattern of the specific energy production from the wind turbine complement the pattern of the PV system specific energy production, especially during the winter months when the PV system production is low due to the high latitude of the selected site (Gothenburg). In particular, the energy production of the wind turbine (30 kW_r) is 24 MWh, whereas the specific production of PV system is 1 MWh/kW_p.

All the hourly climatic data used in this study are coming from a consistent database, Meteonorm [19]. Thus, the effect of both snowy days and rainy days on the solar radiation and thus on the PV power production is intrinsically taken into account. Nevertheless, the effect of the snow on the PV power production during the days after the snow event is not taken into account in this study for several reasons: it is difficult to predict, it is beyond the scope of this study, and the probability of having snow is higher during those months marked out by extremely weak solar radiation. It is worth to say that the effects of snow on the PV system production depends on several factors such as PV array tilt angle, snow texture and depth, and climatic conditions immediately after the snow event. A previous research study evaluated the losses due to snow ranging from 1% to 12% of the total annual energy production for Colorado and Wisconsin [54]. As can be seen from Figure 6, snow event can mostly occur in January, February, March and December. The cumulative solar irradiation of those months represents less than 20% of the total solar irradiation. Thus, it is likely that the snow is going to have a minor contribution on the total energy losses of the PV system

3.3 Water demand and supply

The monthly profile of water consumption and water harvested for a single household is presented in Figure 10.

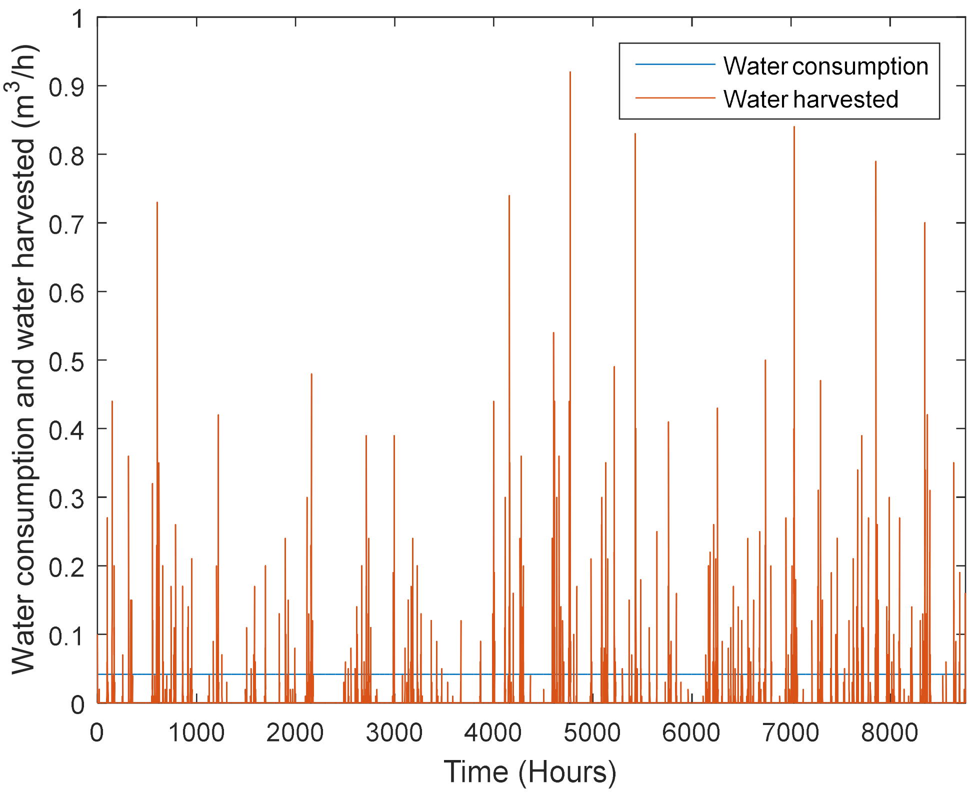

Figure 10: Water consumption and water harvested profile through the year in Gothenburg.

On annual basis a single household of 5 occupants consumes 365 m^3 based on the statistics of the Swedish Water & Wastewater Association [32]. The potential water harvested by a single household considering both precipitation and snow depth is 79.3 m^3/year, about 25% of the annual consumption.

3.4 Optimization results

The results of the GA optimization process regarding the mutual relationship between LCC and reliability of renewables are depicted in Figures 11-13 in the form of a typical Pareto front. The results show that the LCC increase with the increase of the achievable reliability. Moreover, the LCC and reliability are functions of the built environment area and related electric load. A parity of reliability, the LCC increase with the increase of the built environment area due to the high electric load. The system LCC and reliability are also closely dependent on the load to be covered and on the building type. A parity of reliability, the LCC increase passing from case C1 to case C3 considering to cover the electric load of the heat pump for different type of buildings. It has to be noted that for reliabilities equal to zero, the LCC are never equal to zero due to the definition of the LCC function that includes the LCC of electricity bought from the grid for meeting the electric load. It is interesting to note that for low reliabilities the Pareto front shows a slight bending towards lower LCC, see for example Figure 13, S3-C3. This is due to the LCC of electricity produced by renewables is lower than the LCC of electricity bought from the grid. This results is mainly due to the implementation of ground mounted PV systems. Higher reliabilities are guaranteed through the implementation of both building integrated PV systems but mainly through battery storage system that negatively affect the overall LCC. The results show that hybrid renewables based power system can achieve 95% reliability, assuming a built environment area that covers 25% (S1) of the entire study area for case C1. In case the built environment area covers 75% (S3) of the entire 1 km^2, the reliability can achieve 70%. Considering to cover both the electrical demand for appliances and for space heating and cooling (C3), the maximum hybrid power system reliability range between 45% (S3) and 75% (S1). The high latitude of Sweden put a lot of challenges in exploiting solar resources and thus solar PV power. Even more crucial is the mismatch between solar electricity production and electricity consumption. To cope with such issue, hybrid renewable power systems (combination of different renewable based power system) equipped with energy storage can represent a solution, especially for single family households. The results of this study show that high hybrid power system reliabilities are difficultly achieved or are achieved but at high LCC_{ren}, in particular due to the high LCC of the energy storage system. Small-scale wind power system have competitive price compared to PV systems and can balance the weak energy production of PV systems during the winter months. Nevertheless, their integration in residential districts results difficult for problems related to sound and vibration emissions, visual impacts, and turbulence effects that can reduce the energy output.

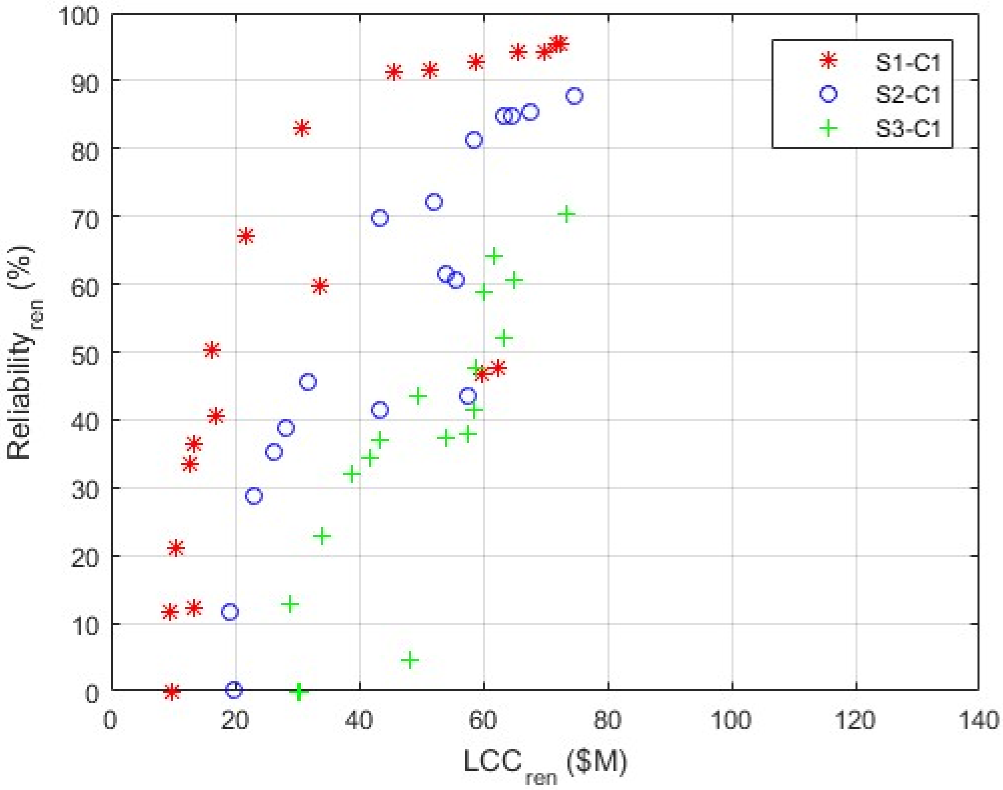

Figure 11: Hybrid power system optimization results for scenarios/case S1/S2/S3-C1.

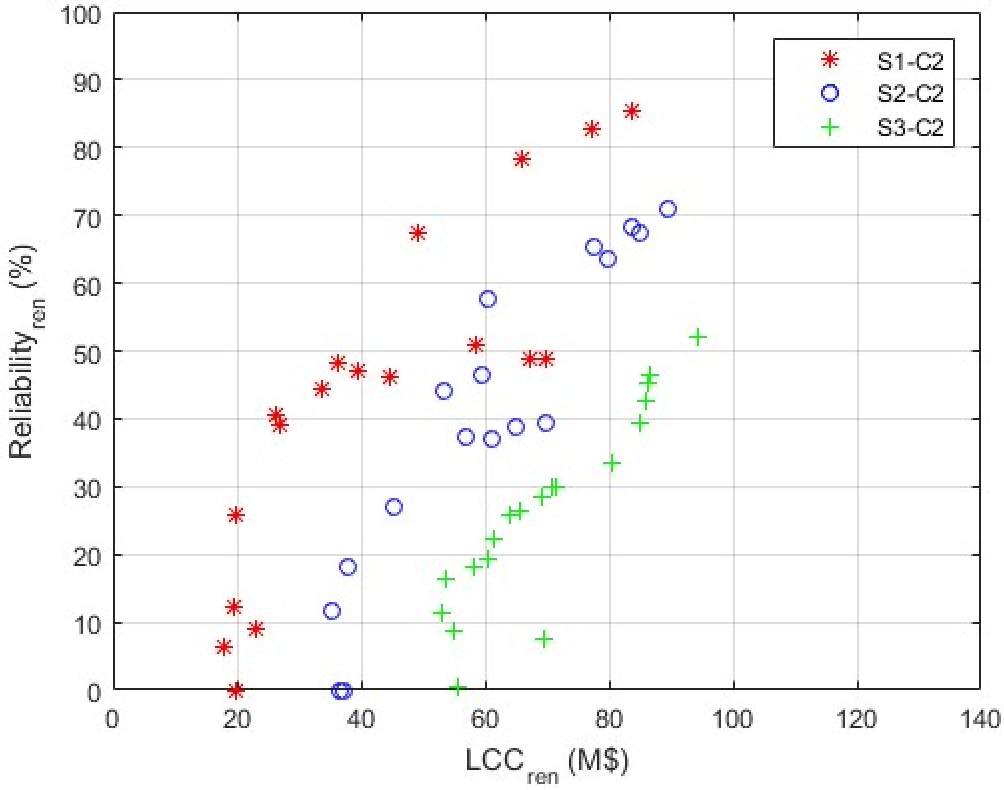

Figure 12: Hybrid power system optimization results for scenarios/case S1/S2/S3-C2.

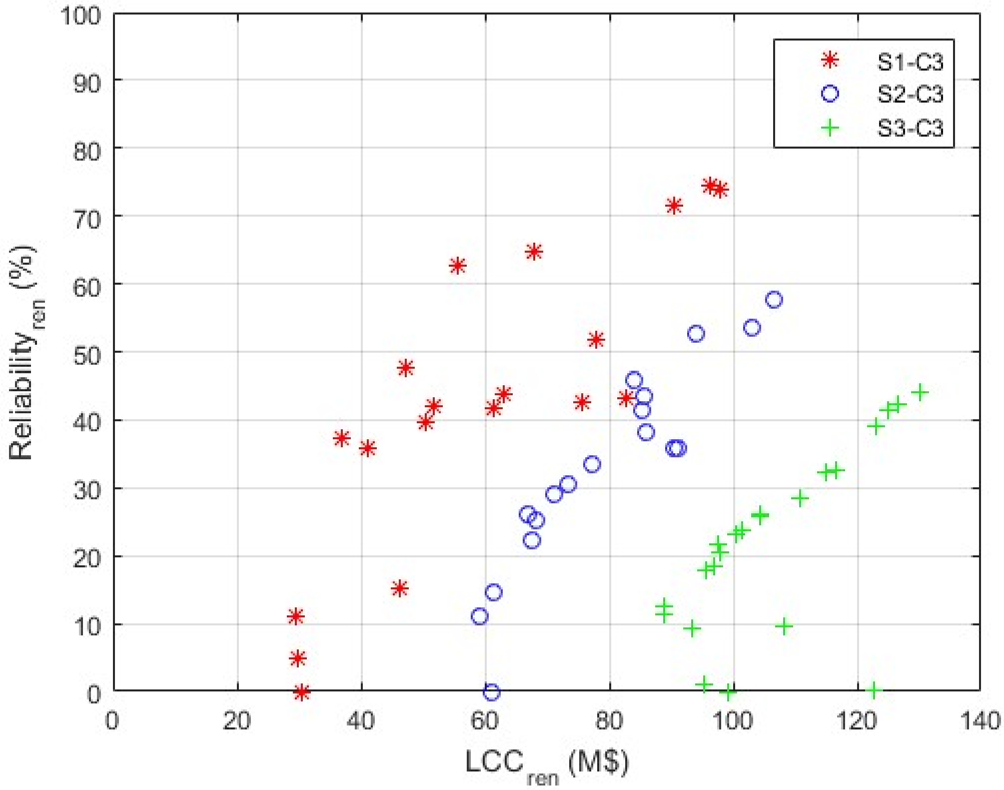

Figure 13: Hybrid power system optimization results for scenarios/case S1/S2/S3-C3.

The GA optimization results regarding the LCC and reliability of the water harvesting system are depicted in Figure 14. Similarly to what investigated for the renewables, the LCC of the water harvesting system increase with the increase of the reliability and built environment area. It is interesting to note that the water harvesting system reliability is always higher than 0, about 5-10%, due to the assumption of using the roof area as part of the total harvester area. At the same time, the LCC are never equal to 0 due to the definition of the LCC function that includes the LCC of water bought from the water network for meeting the buildings water load. Nevertheless, differently to the renewables distribution optimization, the optimization results regarding the water harvesting system are more scattered, especially for the scenarios S1 and S2. This is due to the multi objective nature of the optimization problem. In fact, the objective of increasing the renewables reliability is generally pursued by increasing the PV area, especially ground mounted PV area, and battery capacity. Nevertheless, high renewables reliabilities can be achieved by increasing the battery storage capacity without further increasing the ground mounted PV area. The water harvested depends on the ground PV system area and on the water harvesting system capacity that is an independent variable as well. As a result, the Pareto front is scattered. Taking into consideration scenario S3 the optimal point are more concentrated because the ground mounted PV area is limited due to the high built environment area and higher reliabilities can be achieved with higher water harvesting system capacities but at high LCC. The water harvesting system can meet the water load from 30% to 100% depending on the scenarios considered, S3 and S1 respectively. A summary of the optimization results for the scenario-case S2-C3, renewables and water harvester reliabilities and LCC, surplus of electricity injected into the grid and the corresponding values of the decisional variables is given in Table 7.

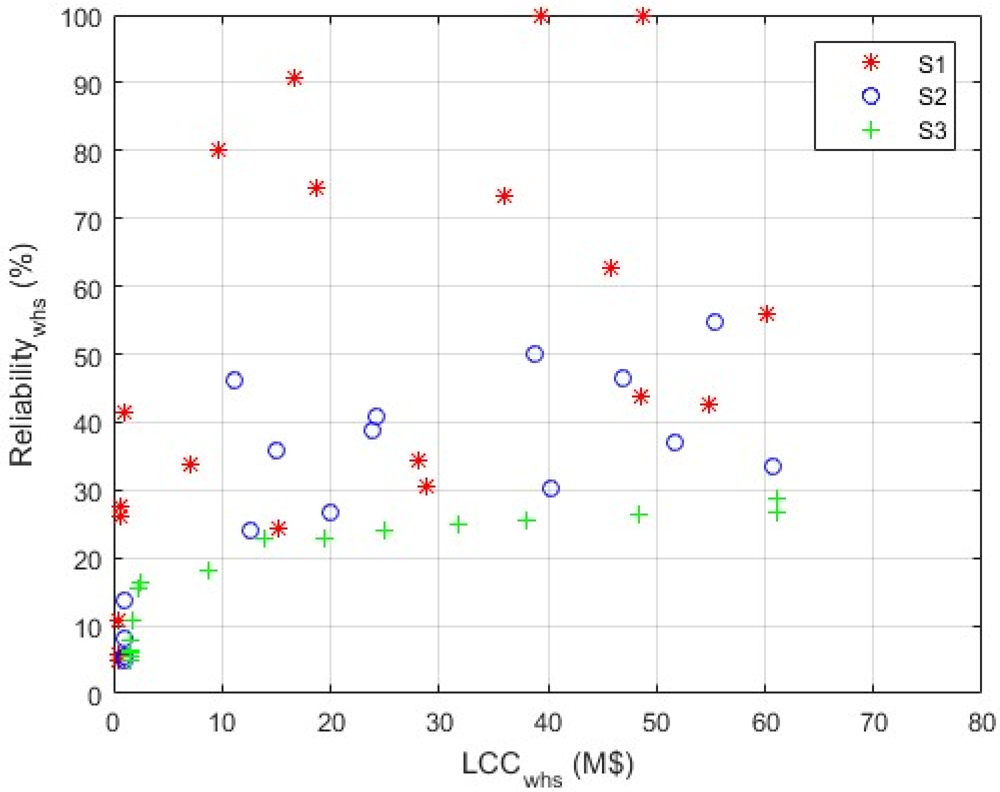

Figure 14: Water harvesting system optimization results for scenarios S1/S2/S3.

Table 7: Optimization results for the scenario-case S2-C3.

LCC_{ren} (M$)	R_{ren} (%)	LCC_{whs} (M$)	R_{whs} (%)	ES (GWh)	ABIPV (km^2)	APV (km^2)	Awind (km^2)	Bc (MWh)	WHc (m^3)
106.622	57.557	34.139	49.909	162.688	0.036	0.330	0.000	7.962	22401.382
102.935	53.676	19.411	47.694	171.367	0.036	0.340	0.000	6.123	12566.558
94.005	52.785	16.705	47.329	131.627	0.009	0.342	0.000	6.488	10759.925
85.520	43.539	53.362	38.790	84.155	0.040	0.138	0.025	4.250	35137.792
85.330	41.438	36.986	44.018	120.941	0.026	0.250	0.000	2.835	24258.901
73.446	30.514	52.945	30.537	43.437	0.040	0.035	0.025	1.785	34801.875
71.209	29.098	12.550	31.553	77.118	0.023	0.152	0.025	0.024	7878.630
68.232	25.160	4.268	21.998	46.518	0.033	0.053	0.000	0.000	2290.031
67.477	22.226	60.754	29.144	32.867	0.040	0.000	0.025	0.000	40000.000
67.477	22.226	60.754	29.144	32.867	0.040	0.000	0.025	0.000	40000.000
67.477	22.226	60.754	29.144	32.866	0.040	0.000	0.025	0.000	40000.000
67.477	22.226	60.754	29.144	32.866	0.040	0.000	0.025	0.000	40000.000
67.053	26.119	45.249	35.137	53.059	0.019	0.112	0.000	0.000	29702.745
61.534	14.566	43.647	27.317	10.331	0.015	0.016	0.000	0.006	28579.600
59.228	11.084	1.009	5.331	5.150	0.000	0.043	0.000	0.000	1.888

In all the presented optimization results, the maximum available area for building integrated photovoltaic systems, equal to 58900 m^2, is never reached since the power produced from ground mounted PV systems is preferred due to the lower LCC costs. Renewables reliabilities higher than 30% are achieved through the implementation of energy storage systems. In most of the optimization results, PV systems are preferred to wind power systems both for economic reason but also for the weak wind potential marking out the case study. The reliability of the water harvesting system are closely connected to the ground mounted PV system area or water harvester capacity. The resulting LCOE for scenario-case S2-C3 are presented in Figure 15 as a function of the reliability and considering subsidies on residential and commercial/utility scale PV systems.

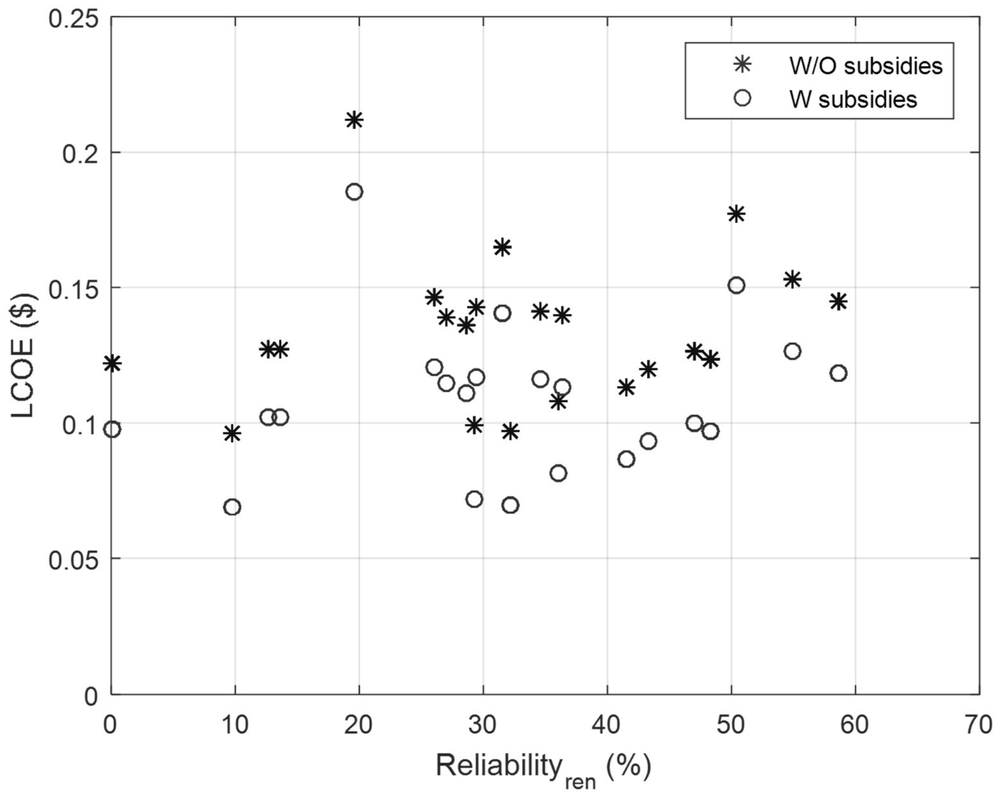

Figure 15: LCOE as a function of the reliability and subsidies.

The LCOE range between 0.096 and 0.212 \$/kWh with a minor tendency to increase at higher reliabilities. Taking into account the subsidies shifts the LCOE range between 0.069 and 0.186 \$/kWh. Obviously, the calculation of the LCOE is closely dependent on several factors, primarily economic but also technical. A sensitivity analysis on how the most significant parameters, such as residential PV system ICC, ground mounted PV system ICC, and battery ICC, can affect the variation of the LCOE for different overall system reliabilities are presented in Figures 16a and 16b, for low (10%) and high (60%) reliability, respectively. The influence of each parameter is studied with a percentage of variation ranging between -/+ 50%. The effects of wind turbine costs on the LCOE have not been investigated due to the results shown in Table 111111 where the wind turbine selection is very limited. At low reliabilities, the ground PV system investment cost has the strongest impact on the LCOE, followed by the building integrated PV system. A variation of 50% for the ground mounted PV system ICC can results in a variation of 40% in the LCOE. The match between power production and consumption allows to achieve low reliabilities without the integration of battery storage systems. This explains why the variation of the battery ICC has no effect on the LCOE variation at low reliabilities. At high reliabilities, the ground mounted PV system ICC still play the key role in affecting the LCOE but in this case even the battery ICC can have a strong impact comparable to the ICC of the building integrated PV system. Despite the battery system increase the LCOE, it has to be highlighted that the LCOE as indicator does not quantify the value of the service provided: the system reliability.

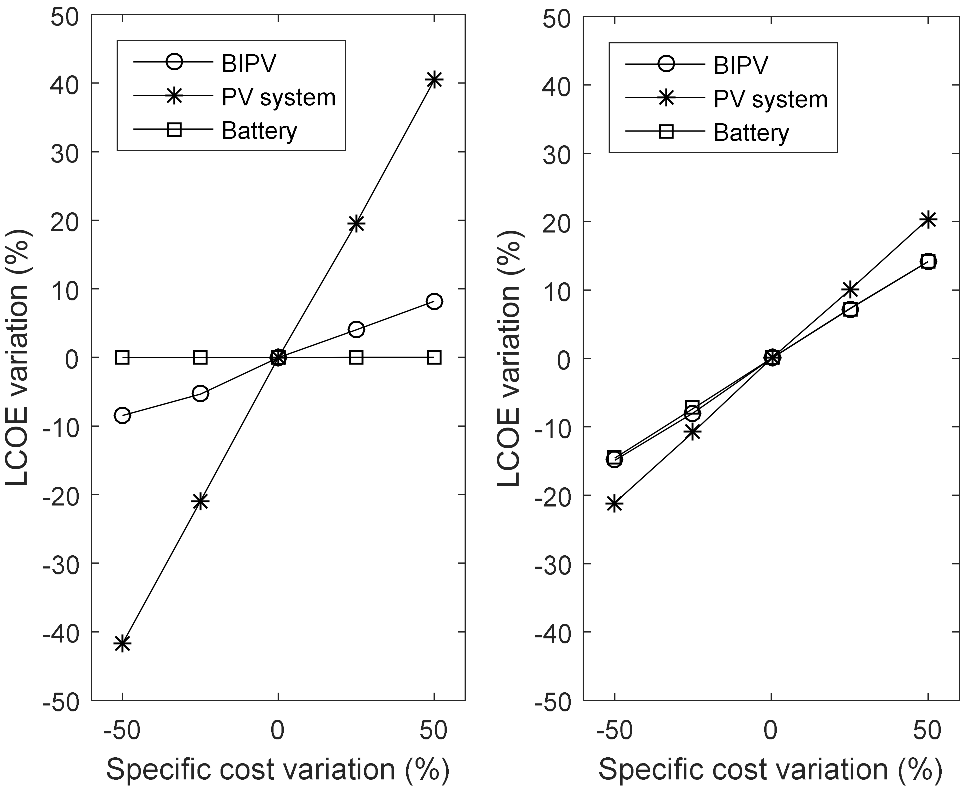

Figure 16: Effects of specific cost variation on the LCOE (a) low reliabilities; b) high reliabilities).

The LCOW as a function of the reliability of the water harvesting system is depicted in Figure 17 together with the main parameters affecting the water harvesting reliability: the building integrated PV area, the ground mounted PV area, and the water harvester volume. For reliabilities below 20% the LCOW is kept below 1$/$m^3$ that is a competitive compared with the water tariff of 1.7 US$/$m^3$. This reliabilities range can be achieved with the roof areas and small scale water harvester tanks, easy to be connected to the building and implemented in residential districts. Higher reliabilities can be achieved through the use of further rainfall harvesting areas and larger scale water harvester tanks with the effect of extremely high LCOW. Similarly for the LCOE, the LCOW cannot quantify the added value for having a water backup. Both for the LCOE and LCOW the results achieved are tightly linked to the particular climatic conditions of the selected site.

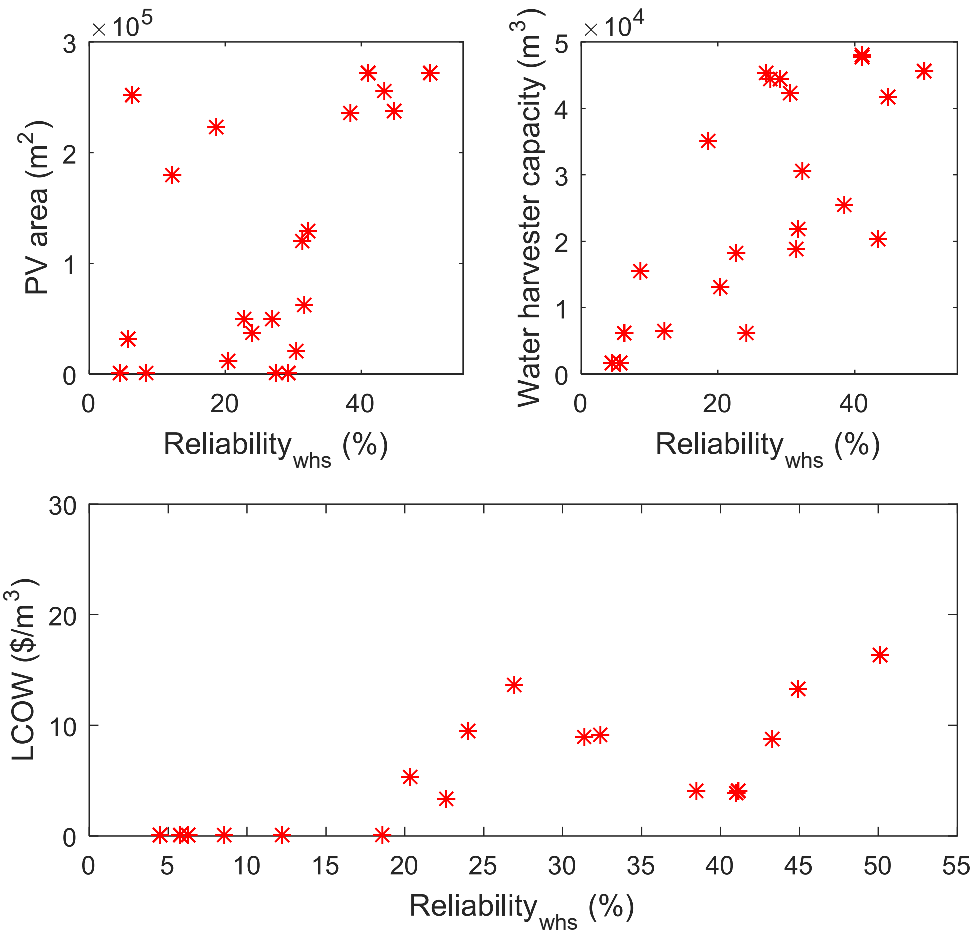

Figure 17: LCOW as a function of water harvesting system reliability, and reliability as a function of ground mounted PV area and water harvester capacity.

As stated at the beginning of this study, the developed model can be used to assess the water and energy performance of existing district or for the planning of new ones. Taking as example the part of residential district studied in Figure 2, the proposed model can be used for evaluating the energy demand and for providing suggestions for improving energy and water performances of the district. A potential improvement scenario of the energy and water efficiency is depicted in Figure18 where the integration of building integrated PV systems, ground mounted PV systems, wind turbine, battery storage, and water harvesting system is implemented. In particular the depicted scenarios shows the integration of both centralized and decentralized energy and water storage systems on a district level. It has to be highlighted that the integration of wind power system and ground mounted PV system has been executed on the public green-leisure area. In the real case, the social and environmental values of the green spaces have to be carefully taken into account but this aspect is beyond the scope of this study.

In this study, we have assumed to use all the rainfall and snow harvested by building roof area and ground mounted effective PV system area to meet the water loads of the households. This assumption may cause an alteration of the hydrological cycle and cause a decline of the groundwater level. These negative effects are connected to the extension of the building area and several other human, climatic and natural factors. Nevertheless, the investigation of these effects is beyond the scope of this article.

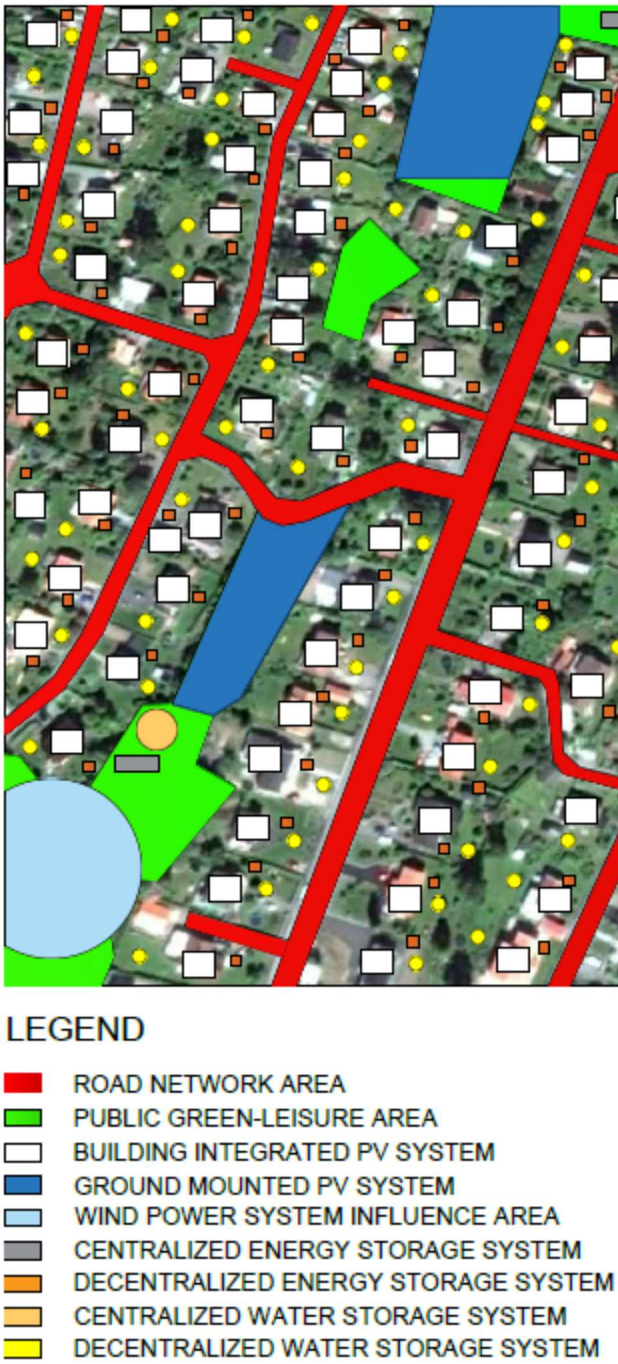

Figure 18: Renewables and water harvesting integration in the residential district.

4 Conclusions

This study present an optimization model to evaluate the optimal area distribution among built environment area, and area for the installation of the renewables to achieve high renewables and water harvesting reliabilities compared to electricity and water loads for a residential district of Gothenburg, Sweden. The optimization process minimizes the life cycle costs of the hybrid renewables based power system and water harvesting systems guaranteeing at the same time their maximum reliabilities. From the result achieved the following conclusions can be drawn:

- The optimization results show that the reliability of the hybrid renewables based power system can vary between 40 and 95% depending on the scenarios considered regarding the built environment area and on the cases concerning the overall electric load.
- The life cycle cost increase with the increase of the achievable hybrid power system reliability. The life cycle cost and reliability are functions of the considered built environment area and related electric load. Assuming the same reliability, the life cycle cost increases with the increase of the built environment area due to the high electric load, and it increases increasing the overall electric load.
- The levelized cost of electricity vary between 0.096 and 0.212 \$/kWh. The levelized cost of electricity is mainly sensitive to the ground mounted PV system specific cost at low reliabilities and to both ground mounted PV system and battery system specific costs at high reliabilities.
- The maximum water harvesting system reliability varies between 30% and 100% depending on the built environment area distribution. For annual reliabilities below 20% the levelized cost of water is kept below 1\$/m^3 making it competitive with the network water tariff.

The developed model will be further developed to also study other type of urban districts. Moreover, other services, such as other renewables and sustainable solutions, wastewater treatment and transportation will be included in the optimization process. Other sites with different climatic conditions will be studied as well.

5 Acknowledgements

This work has been financially supported by KK-stiftelsen through Future Energy Center at Mälardalen University. The authors also thank Wallenstam AB for the financial support.

6 References

[1] World Health Organization, “World health statistics 2014”, 2014. Available from: http://apps.who.int/iris/bitstream/10665/112738/1/9789240692671_eng.pdf. Accessed: 3rd October 2015

[2] United Nations, “The World Population Situation in 2014”, 2015. Available from: http://www.un.org/en/development/desa/population/publications/pdf/trends/Concise%20Report%20on%20the%20World%20Population%20Situation%202014/en.pdf. Accessed: 3rd October 2015

[3] GIZ, ICLEI, “Operationalizing the Urban NEXUS - Towards resource-efficient and integrated cities and metropolitan regions”, 2014. Available from: http://resilient-cities.iclei.org/fileadmin/sites/resilient-cities/files/Full_papers/Urban_NEXUS_Publication_ICLEI-GIZ_2014_web.pdf. Accessed: 3rd October 2015

[4] T. Ma, H. Yang, L. Lu, J. Peng, “Optimal design of an autonomous solar–wind-pumped storage power supply system”, Applied Energy 160 (2015) 728–736

[5] T. Ma, H. Yang, L. Lu, “A feasibility study of a stand-alone hybrid solar–wind–battery system for a remote island”, Applied Energy 121 (2014) 149–158

[6] C. Shang, D. Srinivasan, T. Reindl, “An improved particle swarm optimisation algorithm applied to battery sizing for stand-alone hybrid power systems”, Electrical Power and Energy Systems 74 (2016) 104–117

[7] L.K. Gan, J.K.H. Shek, M.A. Mueller, “Hybrid wind–photovoltaic–diesel–battery system sizing tool development using empirical approach, life-cycle cost and performance analysis: A case study in Scotland”, Energy Conversion and Management 106 (2015) 479–494

[8] A. Maleki, F. Pourfayaz, “Optimal sizing of autonomous hybrid photovoltaic/wind/battery power system with LPSP technology by using evolutionary algorithms”, Solar Energy 115 (2015) 471–483

[9] A. González, J.R. Riba, A. Rius, R. Puig, “Optimal sizing of a hybrid grid-connected photovoltaic and wind power system”, Applied Energy 154 (2015) 752–762

[10] P. García-Triviño, A.J. Gil-Mena, F. Llorens-Iborra, C.A. García-Vázquez, L.M. Fernández-Ramírez, F. Jurado, “Power control based on particle swarm optimization of grid-connected inverter for hybrid renewable energy system”, Energy Conversion and Management 91 (2015) 83–92

[11] Y. Lu, S. Wang, K. Shan, “Design optimization and optimal control of grid-connected and standalone nearly/net zero energy buildings”, Applied Energy 155 (2015) 463–477

[12] S. Carlucci, G. Cattarin, F. Causone, L. Pagliano, “Multi-objective optimization of a nearly zero-energy building based on thermal and visual discomfort minimization using anon-dominated sorting genetic algorithm (NSGA-II)”, Energy and Buildings 104 (2015) 378–394

[13] Y. Lu, S. Wang, Y. Zhao, C. Yan, “Renewable energy system optimization of low/zero energy buildings using single-objective and multi-objective optimization methods”, Energy and Buildings 89 (2015) 61–75

[14] H. Lu, Z. Yu, K. Alanne, L. Zhang, L. Fan, Xu Xu, Ivo Martinac, "Transition path towards hybrid systems in China: Obtaining net-zeroexergy district using a multi-objective optimization method", Energy and Buildings 85 (2014) 524–535

[15] M.H.R. Mehrabadia, B. Saghafian, F.H. Fashi, "Assessment of residential rainwater harvesting efficiency for meeting non-potable water demands in three climate conditions", Resources, Conservation and Recycling 73 (2013) 86– 93

[16] H. Hashim, A. Hudzori, Z. Yusop, W.S. Ho, "Simulation based programming for optimization of large-scale rainwater harvesting system: Malaysia case study", Resources, Conservation and Recycling 80 (2013) 1– 9

[17] Y.R. Chiu, C.H. Liaw, L.C. Chen, "Optimizing rainwater harvesting systems as an innovative approach to saving energy in hilly communities", Renewable Energy 34 (2009) 492–498

[18] S. Mathew, "Wind Energy-Fundamentals, resource analysis and economics", Ed. Springer, 2006

[19] Meteonorm. Available from: www.meteonorm.com. Accessed: 3rd October 2015

[20] M. Cambell, "The Drivers of the Levelized Cost of Electricity for Utility-Scale Photovoltaics", 2008

[21] W. Short, D. Packey, T. Holt, "A Manual for the Economic Evaluation of Energy Efficiency and Renewable Energy Technologies", National Renewable Energy Laboratory – March 1995

[22] Trading economics. Available at: http://www.tradingeconomics.com/. Accessed: 3rd October 2015

[23] IRENA, "Renewable power generation costs in 2014", 2015. Available at: http://www.irena.org/documentdownloads/publications/irena_re_power_costs_2014_report.pdf. Accessed: 3rd March 2016

[24] H. Muyingo, “Organizational challenges in the adoption of building applied photovoltaics in the Swedish tenant-owner housing sector”, Sustainability 2015, 7, 3637-3664

[25] Swedish Energy Agency, “Stöd till solceller”, http://www.energimyndigheten.se/fornybart/solenergi/stod-till-solceller/. Accessed: 9th March 2016 (In Swedish)

[26] J. Hirvonen, G. Kayo, A. Hasan, K. Sirén, “Zero energy level and economic potential of small-scale building-integrated PV with different heating systems in Nordic conditions”, Applied Energy (2016) (In press), doi:10.1016/j.apenergy.2015.12.037

[27] B. Nykvist, and M. Nilsson, “Rapidly falling costs of battery packs for electric vehicles”, Nature Climate Change 2015, doi: 10.1038/nclimate2564

[28] T.R. Gurung, A. Sharma, “Communal rainwater tank systems design and economies of scale”, Journal of Cleaner Production 67 (2014) 26e36

[29] Eurostat, “Energy price statistics”. Available at: http://ec.europa.eu/eurostat/statistics-explained/index.php/Energy_price_statistics. Accessed: 9th March 2016

[30] Nordpool. Available at: http://www.nordpoolspot.com/. Accessed: 9th March 2016

[31] KPMG INTERNATIONAL, “Taxes and incentives for renewable energy”, 2014. Available at: https://www.kpmg.com/Global/en/IssuesAndInsights/ArticlesPublications/Documents/taxes-incentives-renewable-energy-v1.pdf. Accessed: 9th March 2016

[32] The Swedish Water & Wastewater Association, “Facts on water supply and sanitation in Sweden”, 2000. Available from: http://www.svensktvatten.se/Documents/Kategorier/Om%20Svenskt%20Vatten/Facts%20on%20Water%20Supply%20and%20Sanitation%20in%. Accessed: 9th March 2016

[33] K. Deb, A. Pratap, S. Agarwal, T. Meyarivan, “A Fast and Elitist Multiobjective Genetic Algorithm: NSGA-II”, IEEE Transactions On Evolutionary Computation, vol. 6, 2002

[34] I.J. Esfahani, C. Yoo, “An optimization algorithm-based pinch analysis and GA for an off-grid batteryless photovoltaic-powered reverse osmosis desalination system”, Renewable Energy 91 (2016) 233e248

[35] P.E. Campana, H. Li, J. Zhang, R. Zhang, J. Liu, J. Yan, “Economic optimization of photovoltaic water pumping systems for irrigation”, Energy Conversion and Management, vol. 95, p. 32–41, 2015

[36] S.M. Zhang, L. Yang, X.W. Zhao, J.X. Qiang, “A GA optimization for lithium–ion battery equalization based on SOC estimation by NN and FLC”, Electrical Power and Energy Systems 73 (2015) 318–328

[37] X. Chang, M. Dong, D. Yang, “Multi-objective real-time dispatching for integrated delivery in a Fab using GA based simulation optimization”, Journal of Manufacturing Systems 32 (2013) 741–751

[38] Holland J. Adaptation in natural and artificial systems. Cambridge, MA: MIT Press; 1992

[39] S. Wang, X. Xu, “Parameter estimation of internal thermal mass of building dynamic models using genetic algorithm”, Energy Conversion and Management 47 (2006) 1927–1941

[40] S. Sinha, S.S. Chandel, “Review of recent trends in optimization techniques for solar photovoltaic–wind based hybrid energy systems”, Renewable and Sustainable Energy Reviews 50 (2015) 755–769

[41] OptiCE. Available at: www.optice.net. Accessed: 9th September 2016

[42] D. Kalyanmoy. Multi-Objective Optimization Using Evolutionary Algorithms. John Wiley & Sons, 2001

[43] Polysun. Available at: http://www.velasolaris.com/. Accessed: 9th March 2016

[44] S. Berretta, "Feasibility study of using wind power driven heat pump to supply heat for a single house", Master Thesis at Mälardalen University, 2013. Available at: http://www.diva-portal.org/smash/get/diva2:679376/FULLTEXT01.pdf. Accessed: 9th March 2016

[45] ASHRAE, "Handbook of Fundamentals. American Society of Heating, Refrigerating and Air-Conditioning Engineers", Atlanta, 2001

[46] J.A. Duffie, V.A. Beckman, "Solar engineering of thermal processes", 3rd ed. Wiley; 2006.

[47] Photon. Available at: http://www.photon.info/photon_site_db_solarmodule_en.photon. Accessed: 9th March 2016

[48] Jonica Impianti. Available t: http://www.jimp.it/. Accessed: 9th March 2016

[49] E. Pedersen, "Noise annoyance from wind turbines - a review", Naturvårdsverket, 2003. Available from: https://www.naturvardsverket.se/Documents/publikationer/620-5308-6.pdf. Accessed: 3rd October 2015.

[50] T. Ma, H. Yang, L. Lu, J. Peng, "Technical feasibility study on a standalone hybrid solar-wind system with pumped hydro storage for a remote island in Hong Kong", Renewable Energy 69 (2014) 7e15

[51] A. Kaabeche, M. Belhamel, R. Ibtiouen, "Techno-economic valuation and optimization of integrated photovoltaic/wind energy conversion system", Solar Energy 85 (2011) 2407–2420

[52] A.B. Kanase-Patil, R.P. Saini, M.P. Sharma, "Sizing of integrated renewable energy system based on load profiles and reliability index for the state of Uttarakhand in India", Renewable Energy 36 (2011) 2809e2821

[53] N. Agarwal, A. Kumar, Varun, "Optimization of grid independent hybrid PV–diesel–battery system for power generation in remote villages of Uttar Pradesh, India", Energy for Sustainable Development 17 (2013) 210–219

[54] B. Marion, R. Schaefer, H. Caine, G. Sanchez, "Measured and modeled photovoltaic system energy losses from snow for Colorado and Wisconsin locations", Solar Energy 97 (2013) 112–121